JACS JOURNAL OF THE AMERICAN CHEMICAL SOCIETY

Article

Cite This: J. Am. Chem. Soc. 2018, 140, 2085−2092

pubs.acs.org/JACS

# Oriented Films of Conjugated 2D Covalent Organic Frameworks as Photocathodes for Water Splitting

Torben Sick,[†,⊥] Alexander G. Hufnagel,[†,⊥] Jonathan Kampmann,[†,⊥] Ilina Kondofersky,[†] Mona Calik,[†] Julian M. Rotter,[†] Austin Evans,[†] Markus Döblinger,[†] Simon Herbert,[†] Kristina Peters,[†] Daniel Böhm,[†] Paul Knochel,[†] Dana D. Medina,[†] Dina Fattakhova-Rohlfing,[*,‡,§] and Thomas Bein[*,†]

[†]Department of Chemistry and Center for NanoScience (CeNS), University of Munich (LMU), Butenandtstraße 5-13, 81377 Munich, Germany

[‡]Institute of Energy and Climate Research (IEK-1) Materials Synthesis and Processing, Forschungszentrum Jülich GmbH, Wilhelm-Johnen-Straße, 52425 Jülich, Germany

[§]Faculty of Engineering and Center for Nanointegration Duisburg-Essen (CENIDE), University of Duisburg-Essen, Lotharstraße 1, 47057 Duisburg, Germany

Supporting Information

**ABSTRACT:** Light-driven water electrolysis at a semiconductor surface is a promising way to generate hydrogen from sustainable energy sources, but its efficiency is limited by the performance of available photoabsorbers. Here we report the first time investigation of covalent organic frameworks (COFs) as a new class of photoelectrodes. The presented 2D-COF structure is assembled from aromatic amine-functionalized tetraphenylethylene and thiophene-based dialdehyde building blocks to form conjugated polyimine sheets, which $\pi$-stack in the third dimension to create photoactive porous frameworks. Highly oriented COF films absorb light in the visible range to generate photoexcited electrons that diffuse to the surface and are transferred to the electrolyte, resulting in proton reduction and hydrogen evolution. The observed photoelectrochemical activity of the 2D-COF films and their photocorrosion stability in water pave the way for a novel class of photoabsorber materials with versatile optical and electronic properties that are tunable through the selection of appropriate building blocks and their three-dimensional stacking.

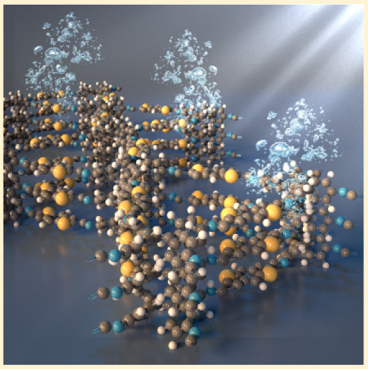

## INTRODUCTION

Photoelectrochemical (PEC) water splitting is an attractive way to generate hydrogen using renewable energy. Due to the potential of directly converting solar power into a chemical fuel or process feedstock, this process has attracted broad research interest. An ideal photoabsorber will combine efficient light harvesting with suitable band energies for water oxidation and reduction, fast interfacial charge transfer kinetics to the electrolyte, and corrosion stability under operating conditions.[1] However, the performance of known systems is modest, being primarily limited by photoabsorber material properties. On the one hand, metal oxides tend to be stable under operation (i.e., resistant against photocorrosion) but exhibit poor semiconductor properties such as short charge carrier diffusion lengths and fast recombination, which can be partially compensated by nanostructuring.[2−4] On the other hand, Si and III−V semiconductors offer favorable charge transport properties and high photocurrents but are prone to photocorrosion unless protected by overlayers.[5,6] For this reason, the discovery of new photoabsorber materials is urgent and currently the focus of combinatorial synthetic and computational research.[7−10]

In this work we explore covalent organic frameworks (COFs) as photoelectrodes for light-driven water splitting. COFs are an emerging class of crystalline polymers composed of organic units linked via covalent bonds to form porous networks. By using multidentate building blocks, two- or three-dimensional frameworks with a defined pore size and high specific surface area in conjunction with appreciable thermal and chemical stability can be obtained. In 2D-COFs, covalently bonded units form two-dimensional (2D) sheets, which stack due to dispersive forces ($\pi$-stacking) in the third dimension to construct extended open porous frameworks. The $\pi$-stacking mediates electronic interactions between the functional units, thereby providing another possible path for charge carrier transport in addition to transfer within the covalent sheets. The selection of appropriate building blocks, linkage motifs (from unconjugated boroxines, boronate esters, and borosilicates[11−14] to conjugated imines,[15−19] imides,[20,21] and others[22−24]), and their stacking mode all provide ways to tailor the optical and electronic properties of COF structures, thereby opening the way for the discovery of novel materials for optoelectronic systems. COFs have found applications in gas storage,[25,26] catalysis,[27,28] separation,[29−31] energy storage,[32] and proton conduction.[33] Zeolitic imidazolate frameworks (ZIFs),[34] carbon

Received: June 14, 2017
Published: December 17, 2017




DOI: 10.1021/jacs.7b06081
J. Am. Chem. Soc. 2018, 140, 2085−2092

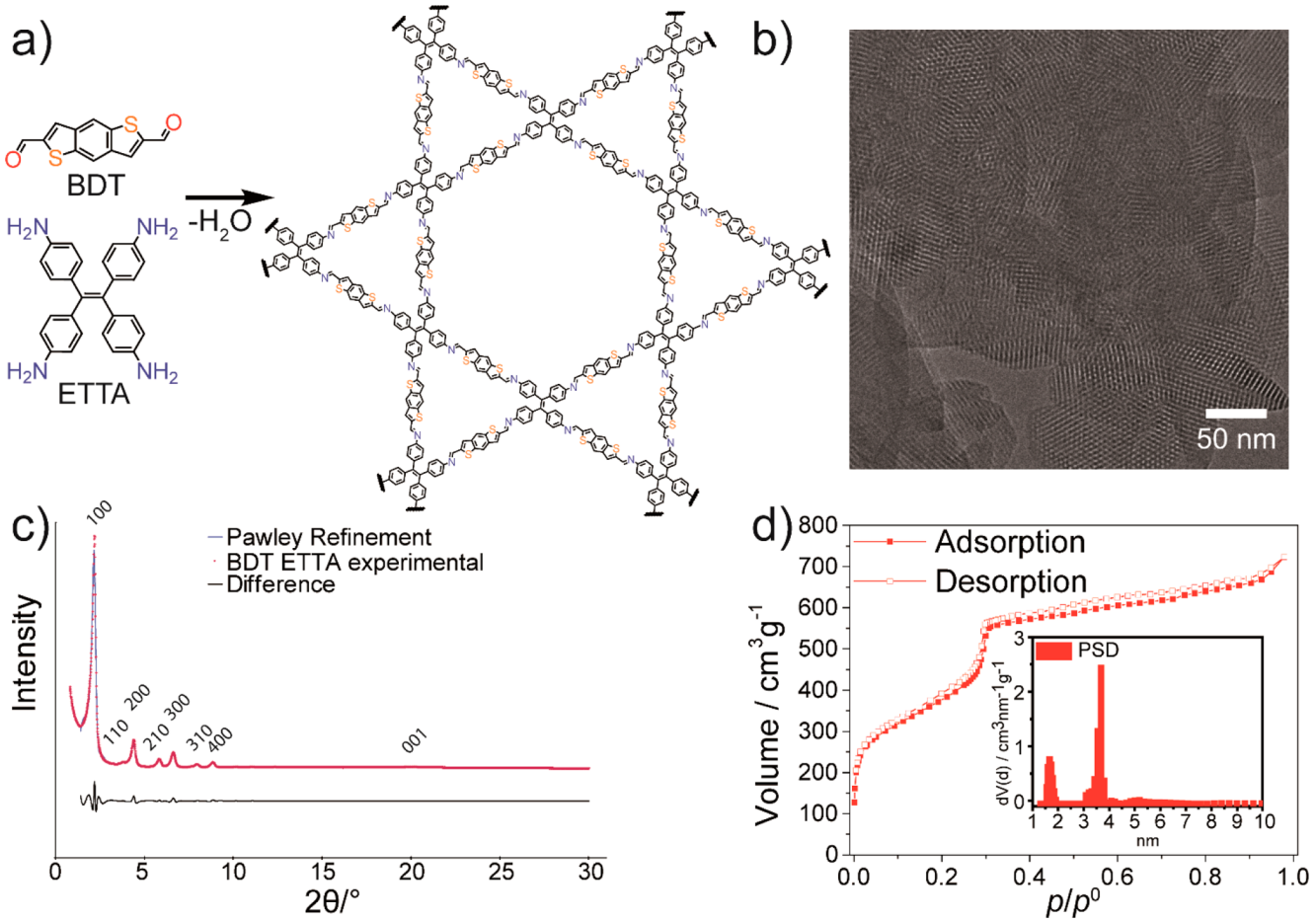


**Figure 1.** (a) Synthetic approach for the formation of a BDT-ETTA COF with a structural overview of the resulting 2D layers. Due to $\pi$-interactions, the sheets stack in the third dimension to form the final hexagonal AA eclipsed framework. (b) TEM image of the resulting powder. (c) PXRD of BDT-ETTA (red), comparison to a Pawley-refined pattern (blue), and difference (black line). (d) Nitrogen physisorption isotherm of BDT-ETTA with a pore size distribution revealing two distinct pore sizes.

nitrides (CNs),[35−40] phenyl triazine oligomers (PTOs),[41] poly(azomethine) networks (ANWs),[42] triazine-containing organic frameworks (CTFs), and even covalent organic frameworks[43−50] were found to be active in photocatalysis and photocatalytic hydrogen evolution reactions, where photogenerated charge separation was achieved by adding noble metal cocatalysts and/or sacrificial electron donors. Fabricated as oriented COF thin films, COFs have already found use as active materials in optoelectronic devices.[51−54] However, COF films being utilized as photoelectrodes for direct water splitting have yet to be reported. Herein, we demonstrate the use of an imine-based COF, grown as oriented film on transparent, conducting substrates, serving as a light-absorbing material. This is the first report of a COF acting as a photoelectrode to enable photoelectrochemical water splitting in aqueous electrolytes without the use of a cocatalyst or sacrificial agent. In addition, we demonstrate a 4-fold increase in the obtained photocurrent by the application of a Pt nanoparticle hydrogen evolution catalyst.

## RESULTS AND DISCUSSION

**Synthesis of COF Systems.** For the possible use as photocathodes in photoelectrochemical watersplitting devices, we investigated a 2D-COF built from aromatic amino- and thiophene-based units. The use of nearly planar p-type functional building units linked via polarizable imine bonds is expected to result in conjugated p-type semiconductors, whose optoelectronic properties can be varied via the structure of the building units and the nature of their stacking in the third dimension.

One building unit is a conjugated aromatic and 4-fold amine-functionalized tetraphenylethylene (1,1′,2,2′-tetra-*p*-aminophenylethylene, ETTA). The ETTA monomer has been investigated in 2D-imine COF powders,[55] where it was shown to have a strong impact on geometry, shape, crystallinity, and the stacking distance of adjacent layers. The other component is the linear dialdehyde benzo[1,2-*b*:4,5-*b*′]-dithiophene-2,6-dicarboxaldehyde (BDT), which is a donor-type dithiophene (Figure 1a).

For use as electrodes in photoelectrochemical cells, the COFs were grown as films on transparent conducting fluorine-doped tin oxide (FTO) or indium tin oxide (ITO) substrates. We found that high concentrations of reactants result in homogeneous nucleation and growth of bulk COF powders, whereas dilute solutions promote heterogeneous film growth on a substrate. To avoid nucleation and precipitation of COF powders on the substrate, the substrates were placed with the FTO or ITO side down in a polytetrafluoroethylene (PTFE) film holder in a mesitylene−benzyl alcohol (v/v = 1:1) solution in an autoclave. After adding a catalytic amount of 6 M acetic acid, the films were grown for 72 h at 120 °C. Intensely orange-colored BDT-ETTA COF films were obtained on FTO or ITO


DOI: 10.1021/jacs.7b06081
J. Am. Chem. Soc. 2018, 140, 2085−2092

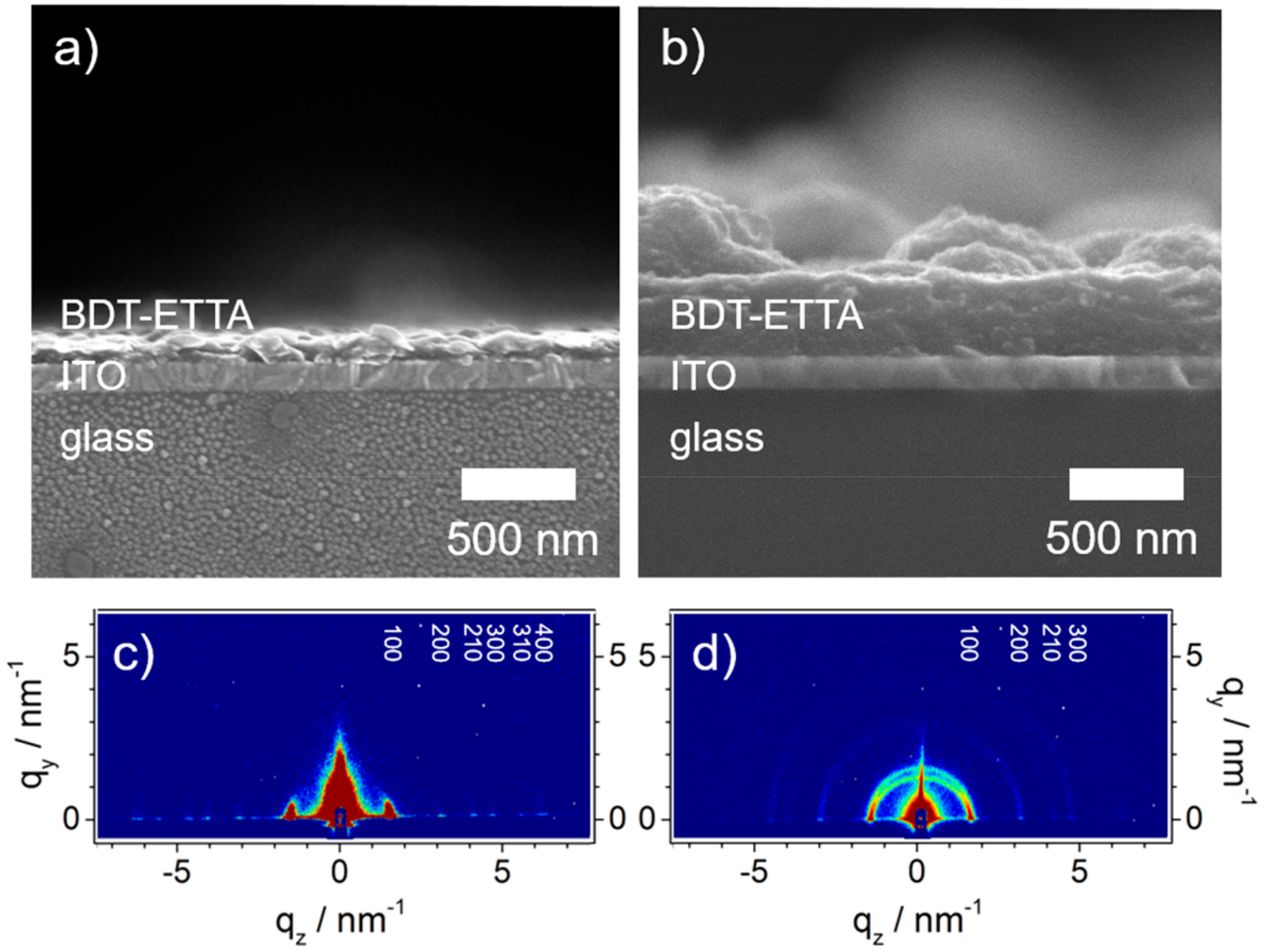


**Figure 2.** Thin (ca. 100 nm) (a, c) and thick (ca. 500 nm) (b, d) BDT-ETTA films grown on ITO substrates: SEM images (cross-section) (a, b) and grazing incidence diffraction (GID) patterns (c, d) revealing a high degree of film orientation.

substrates. Cross-sectional SEM images of BDT-ETTA films (Figure 2) with different thicknesses demonstrate that COF films can be grown in the thickness range between 100 and 500 nm and that they adhere well to the substrate. The surface exhibits some roughness, which is notably less pronounced in the case of thinner films (compare Figure 2a).

The BDT-ETTA COF is crystalline, as established by an intense and sharp 100 reflection and the presence of well-defined higher-order reflections in the powder X-ray diffraction (PXRD) pattern (Figure 1c). The reflection at around 20° 2$\theta$ represents the $\pi$-stacking distance, which corresponds to 0.44 nm. The obtained PXRD pattern agrees well with the simulated pattern calculated for an AA eclipsed layer stacking model for a hexagonal structure in *P*6 symmetry (see Figure 1c and SI Figure 13). The $\pi$-stacking distance is high in comparison to other COF systems, which can be explained by the strong contribution of the propeller-shaped (i.e., nonplanar) ETTA motif to the final geometry compared to the planar thiophene linker.[19]

Notably, both the XRD measurements in reflection mode (SI Figure 11) and grazing incidence diffraction (GID) patterns (Figure 2c,d) provide strong evidence for oriented growth of the COF films on the substrates. The orientation in the *c*-direction is evident from the intense reflections at $q(y) = 0$ originating from COF layers oriented parallel to the substrate and correspond to the reflections of the BDT-ETTA COF (compare PXRD in Figure 1c). A weak diffuse arc arises from randomly distributed COF particles present on top of the highly oriented film (see SI Figures 9 and 11). For the electrochemical investigations we used the thinner films, as they constitute a well-defined system with less non-oriented COF material.

The nitrogen physisorption isotherms of the COF powder demonstrate that the BDT-ETTA COF forms a porous structure with clearly distinguishable micro- and mesopores (Figure 1d). The BET surface areas and total pore volumes for COF bulk material were calculated to be 1360 m$^2$ g$^{-1}$ and 1.0 cm$^3$ g$^{-1}$, respectively. The bimodal pore size distribution shows pores of 1.67 and 3.68 nm in diameter. The pore sizes match the predicted values for the geometry of an AA eclipsed framework.

The TEM image of BDT-ETTA (Figure 1b) reveals a high degree of crystallinity and order, as demonstrated by the large domain sizes. 2D honeycomb-type facets are visible, where the *ab* plane is oriented perpendicular to the viewing direction. In other viewing directions, channels indicate the growth orientation, highlighting the crystallinity of the COF material with domain sizes of 50−100 nm.

**Photoelectrochemical Properties of COF Films.** The remarkable stability of the obtained BDT-ETTA in different


DOI: 10.1021/jacs.7b06081
*J. Am. Chem. Soc.* 2018, 140, 2085−2092

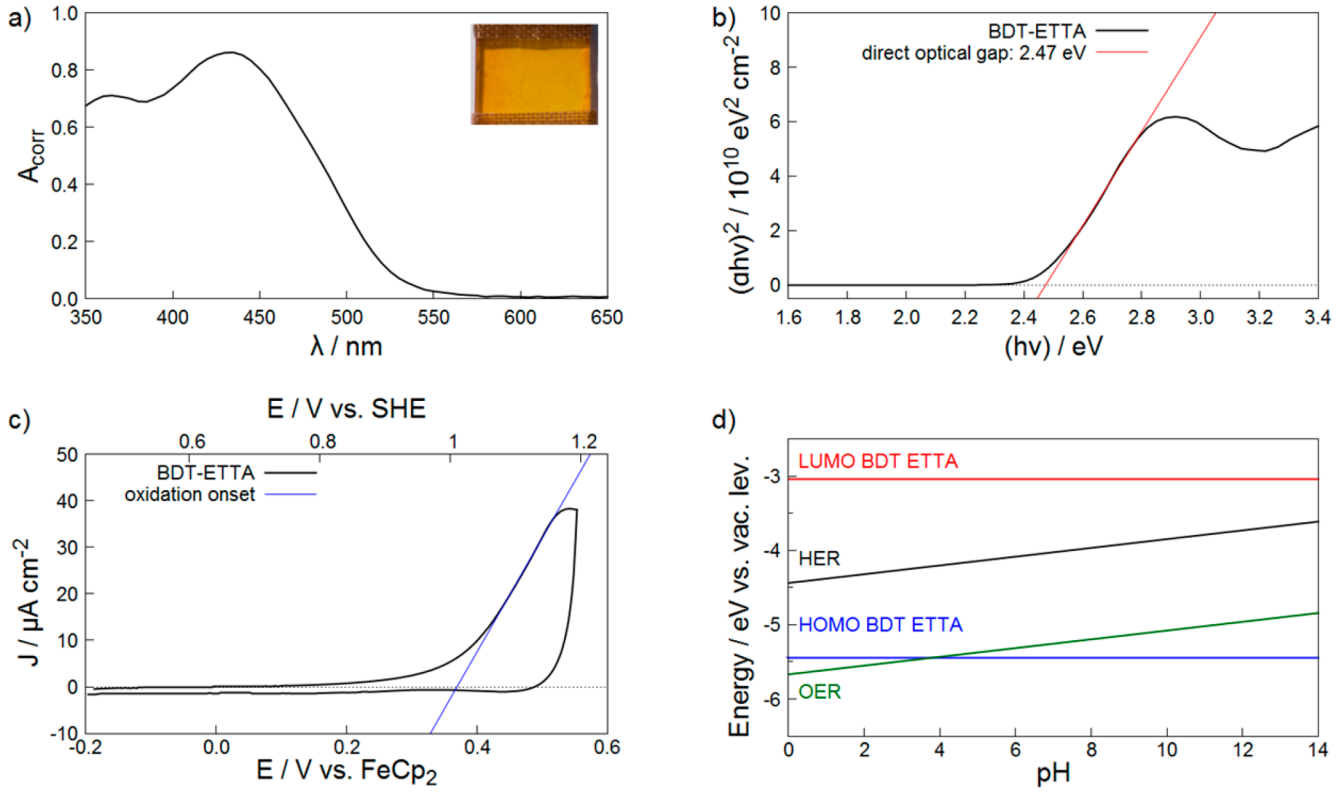


**Figure 3.** (a) Absorbance spectrum of a BDT-ETTA thin film on ITO with a photograph of a representative sample masked with a PFTE adhesive tape (inset). (b) Tauc plot analysis of a BDT-ETTA film on ITO showing a direct optical band gap of 2.47 eV. (c) Cyclic voltammogram of a BDT-ETTA electrode in nonaqueous electrolyte. (d) Calculated alignment between the HOMO and LUMO of BDT-ETTA and the watersplitting redox couples.

solvents, including water in a pH range from 3 to 14 (see SI Figure 12 for further details), and strong absorption of visible light suggested that the novel BDT-ETTA COF structure would be an interesting example of a photoabsorber material for watersplitting applications. Therefore, we measured the photochemical activity at pH 7.

The absorption spectrum is shown in Figure 3. BDT-ETTA films strongly absorb light in the visible range with an absorption threshold of around 550 nm and two absorbance maxima at 360 and 430 nm (Figure 3a). The Tauc plot analysis of BDT-ETTA thin films (Figure 3b) reveals a direct optical band gap of 2.47 eV, which is favorable for photoelectrochemical water splitting.[2]

To determine the absolute positions of the conduction and valence band edges of BDT-ETTA films (corresponding to their LUMO and HOMO energies, respectively), electrochemical measurements in a nonaqueous electrolyte (0.1 M $NBu_4PF_6$ in anhydrous acetonitrile) were performed. The cyclic voltammogram of a BDT-ETTA film electrode (Figure 3c) shows an anodic peak with an onset at 0.37 V vs ferrocene/ferrocenium (FOC), which we attribute to the expected oxidation of thiophene moieties. From this, the approximate position of the HOMO can be calculated to be −5.51 eV (see SI for further details). Using the optical band gap of 2.47 eV determined above, the LUMO position is approximately −3.34 eV. The absolute energy of the HOMO and LUMO of BDT-ETTA as well as the $H_2O/H_2$ (hydrogen evolution reaction, HER) and $O_2/H_2O$ (oxygen evolution reaction, OER) redox couples are plotted in Figure 3d. If we assume that the HOMO and LUMO positions do not change significantly due to protonation or deprotonation of the COF structure, the LUMO is higher in energy than the $H_2O/H_2$ redox pair in solution over the entire pH range, which means that photoexcited electrons at the COF surface should be able to spontaneously transfer to the electrolyte, resulting in proton reduction and hydrogen evolution. The driving force, i.e., the potential difference between the LUMO of the COF and the HER, is significant, particularly in acidic solutions. In alkaline solutions, the HOMO energy lies below that of the OER redox couple, which would also render photoelectrochemical water oxidation and thus bias-free one-photon watersplitting thermodynamically feasible. However, the potential difference is limited to approximately 0.5 V, which approaches the minimum overpotential needed to drive the OER. Therefore, in the absence of an efficient OER catalyst, this reaction is not expected to yield significant currents. The photoelectrochemical performance of 100 nm BDT-ETTA films was characterized by linear sweep voltammetry in nitrogen-purged 0.1 M $Na_2SO_4$ aqueous electrolyte under AM 1.5 illumination through the substrate in the potential range between 1.1 and 0.2 V vs RHE (Figure 4a). The photoelectrode shows an early HER onset potential of 1.0 V vs reversible hydrogen electrode (RHE), reaching currents of up to 1.5 $\mu A\ cm^{-2}$ at 0.2 V vs RHE. We note that thicker (500 nm) films with a less homogeneous orientation (cf. Figure 2b) show a higher current density of 4.3 $\mu A\ cm^{-2}$ at 0.3 V vs RHE, demonstrating that the PEC performance of the COF films can be improved (SI Figure 2). We investigated the cause of the photoactivity using electrodes made by drop-casting the COF components BDT and ETTA individually on ITO substrates. Cyclic voltammograms of these are shown in SI Figure 3. ETTA shows no difference between dark and light currents below 0.4 V vs RHE,


DOI: 10.1021/jacs.7b06081
J. Am. Chem. Soc. 2018, 140, 2085−2092

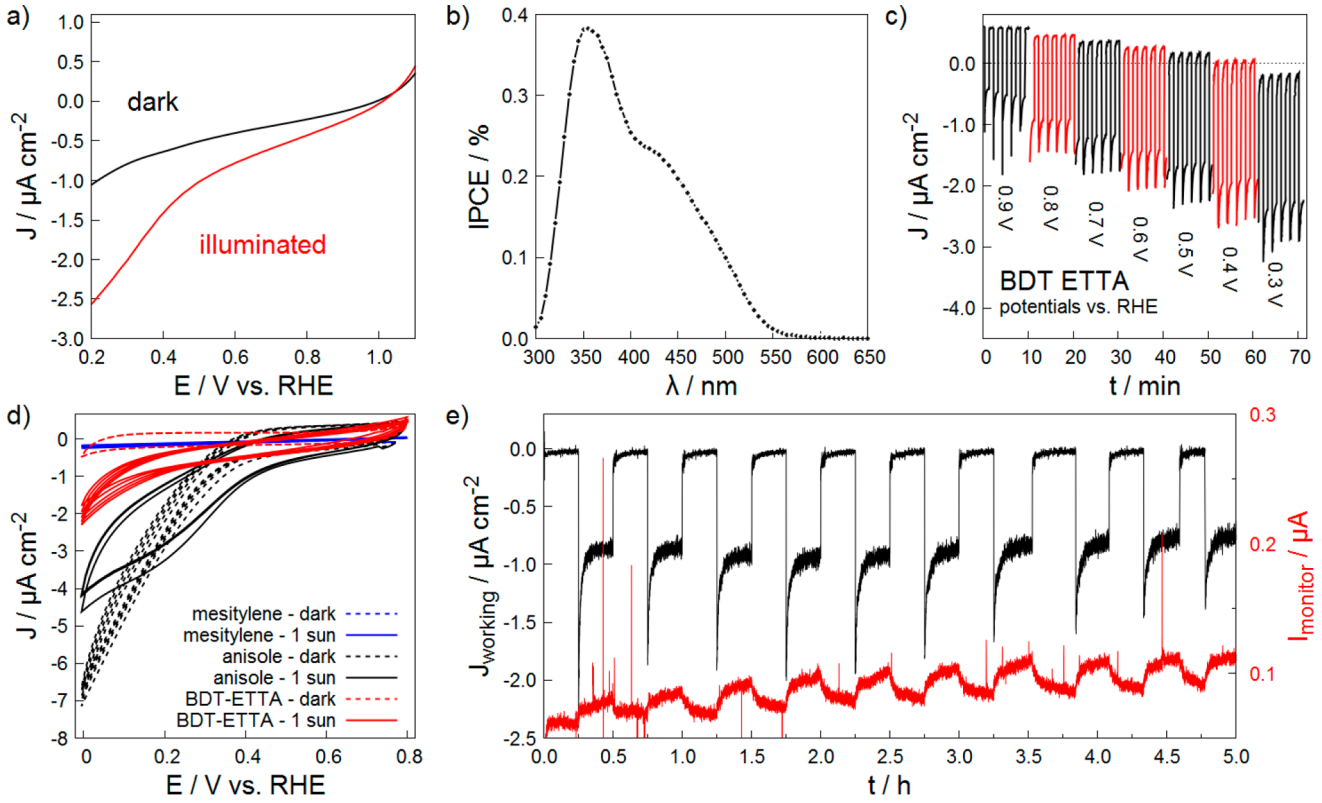


**Figure 4.** (a) Linear sweep voltammograms of BDT-ETTA films on ITO performed in the dark (black) and under AM 1.5 illumination through the substrate (red). (b) The corresponding IPCE spectrum quantifies the photoresponse of the COF electrodes in the visible spectral range. (c) Chronoamperometric data of a BDT-ETTA film collected under chopped illumination (8.3 mHz, 455 nm, $10^{17}$ $s^{-1}$ $cm^{-2}$) demonstrating the photocurrent response at different potentials. (d) Cyclic voltammograms of BDT-ETTA films grown from different solvents. (e) Chronoamperometric data recorded on a BDT-ETTA film at 0.4 V vs RHE (black) under chopped AM 1.5 illumination. Oxidation current recorded simultaneously on a platinum mesh indicator electrode (red) indicating the formation of hydrogen under illumination (see SI for experimental details).

indicating that it is not photoactive by itself. The BDT electrode shows similar but lower photoactivity compared to the COF. We assume, therefore, that the photoactivity of the COF arises from the BDT component and that the formation of an oriented film in which the BDT is covalently bound amplifies its photoresponse and also improves stability. We also investigated whether the oriented porous structure of the BDT-ETTA films is required for successful water reduction. To this end, we prepared reference films using different solvents (mesitylene or anisole) for the COF growth solution, which do not result in oriented growth. Figure 4d shows cyclic voltammograms of these films under dark and illuminated conditions. In the case of films grown from mesitylene, no significant currents are observed in either case. Films grown from anisole exhibit very high dark reduction currents above the HER onset potential, indicating a reaction of the film material. The subsequent cyclic voltammetry scans under illumination yield a photocurrent lower than the original dark current over a wide potential range. This indicates that the film is neither photoactive nor stable under operating conditions. From these findings we conclude that oriented BDT-ETTA films, grown using suitable procedures such as those described in this study, are required for stable water photoreduction. Therefore, due to the well-defined geometry of the highly oriented thin (100 nm) films, we have chosen these as a system for further photoelectrochemical study. The incident-photon-to-current-efficiency (IPCE) of these thin films was determined to examine the photoelectrochemical performance of the COF electrode at different wavelengths (Figure 4b). The BDT-ETTA COF showed light-to-current conversion activity over a broad spectral range below 530 nm, reaching a maximum IPCE of 0.38% at 355 nm. Stability of the photoabsorber is a key requirement for achieving energy payback via photoelectrochemical hydrogen generation.[56] To investigate this issue, we performed chronoamperometric measurements under chopped illumination (8.3 mHz, 455 nm, $10^{17}$ $s^{-1}$ $cm^{-2}$) at different potentials between 0.9 and 0.3 V vs RHE for 10 min each (Figure 4c). BDT-ETTA films showed a stable photocurrent response over the entire potential range, while the absolute values of current density followed the trend of the linear sweep voltammograms.

Further, we investigated the stability of the COF photoelectrode for an extended period of time at 0.4 V vs RHE. At this potential, the BDT-ETTA films showed stable behavior with a negligible dark current density and good photoactivity. Chronoamperometric data were recorded at this potential for 5 h (Figure 4e, black). The sample was alternatingly kept in the dark and illuminated with AM 1.5 simulated sunlight for 15 min at a time. After the initial switch-on transient a steady-state photocurrent density of 0.9 $\mu$A $cm^{-2}$ was reached in each illumination step. To ensure that the resulting photocurrent arises from the water reduction, we designed a four-electrode setup enabling the continuous monitoring of the hydrogen evolution during this stability test (see experimental details and SI Figure 4 for further information). A platinum indicator electrode was placed next to the photocathode and polarized at


DOI: 10.1021/jacs.7b06081
J. Am. Chem. Soc. 2018, 140, 2085−2092

1.1 V vs RHE to oxidize dissolved hydrogen in the electrolyte. An oxidation current recorded at this electrode indicates hydrogen evolution in the system, although quantification of the hydrogen amount via this method is challenging due to a low collection efficiency of the indicator electrode (SI Figure 6). Prior to measurements the indicator electrode was polarized without illumination until a stable background current of 0.06 $\mu$A was reached (SI Figure 5). Illumination of the COF film resulted in a photocurrent detected at the photoelectrode (Figure 4e, black) and a simultaneous rise in the hydrogen oxidation current at the indicator electrode (Figure 4e, red). Switching off the light results in a decay of the photocurrent as well as the oxidation current. This behavior is stable and repeatable over the course of the measurement, indicating stability of the material under photoelectrochemical operating conditions. In order to rule out that the oxidative current observed in Figure 4e results from any other species than photoelectrochemically evolved hydrogen, we quantified the product with a hydrogen microsensor (Unisense A/S $H_2$-NPLR) with a hydrogen-selective silicone membrane. At a static potential of the COF film of 0.4 V vs RHE, a direct correlation between the hydrogen evolution and the illumination of the sample with AM 1.5 simulated sunlight is evident (SI Figure 8). The long-term stability demonstrated by the COF photoelectrode shows that no components of the COF material are dissolved by photocorrosion. This demonstrates that a BDT-ETTA covalent organic framework can be used as a stable photocathode for PEC water reduction. The conversion efficiency of photoelectrodes can be enhanced by a number of methods, including the application of a cocatalyst that facilitates the charge transfer to the electrolyte. We demonstrate that this is viable for COF photocathodes by decorating the COF film with platinum nanoparticles. As shown in Figure 5, the BDT-ETTA/Pt films show a 4-fold increase in photocurrent compared to bare BDT-ETTA photocathodes. Therefore, we see the potential to improve the efficiency of COF photoelectrodes by combining them with suitable cocatalysts.

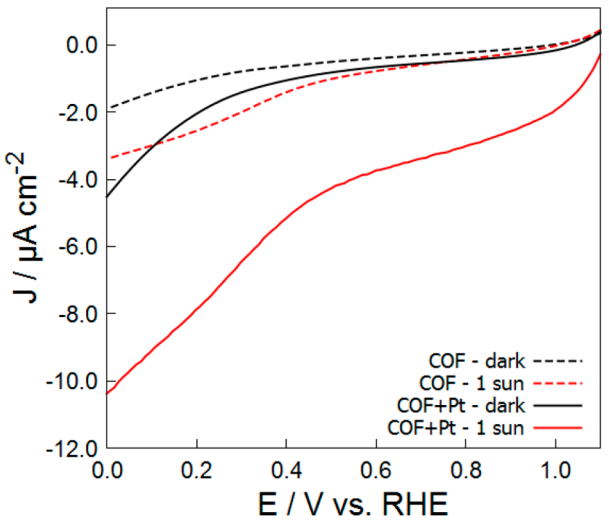


**Figure 5.** Linear sweep voltammograms of BDT-ETTA films on ITO performed in the dark (black) and under AM 1.5 illumination through the substrate (red). The combination of BDT-ETTA with platinum nanoparticles (solid lines) leads to an increased photocurrent over the whole potential range compared to bare BDT-ETTA films (dashed lines).

## CONCLUSION

Our results show that BDT-ETTA COF films are viable photocathodes for light-driven water reduction. The material meets the requirements for this application, which include efficient light harvesting, suitable band positions, and stability. The polyimine framework BDT-ETTA is the first to be investigated in this context, representing an unexplored field of applications for COFs. Given the enormous diversity of molecular building units that can be employed in the construction of COFs, both the development of new framework structures and fine-tuning the properties of existing ones are possible. We envision that future research on combinations of building blocks and stacking modes and the combination of the photoabsorber with suitable cocatalysts will allow for further optimizing charge carrier lifetimes, long-term stability, and charge transfer kinetics in order to improve the conversion efficiency obtainable from COF-based photoelectrodes.

## EXPERIMENTAL SECTION

All reagents and solvents were obtained from commercial suppliers and used as received: benzo(1,2-*b*:4,5-*b*′)dithiophene (>98%, TCI), benzyl alcohol (BnOH, anhydrous, Sigma-Aldrich), mesitylene (Mes, anhydrous, Sigma-Aldrich), tetrahydrofuran (THF, extra dry, stabilized, Acros Organics), acetonitrile (Sigma-Aldrich), ITO glass substrates (Visiontek, 12 Ω/sq), FTO-coated glass substrates (Pilkington, 7 Ω/sq).

**General Procedure for BDT-ETTA COF Films.** Under argon, BDT (7.88 mg, 0.032 mmol) and ETTA (76.28 mg, 0.016 mmol) were finely ground, added to a PTFE autoclave, and suspended in a mixture of benzyl alcohol and mesitylene (v/v 1:1, 2000 $\mu$L). A glass slide holder, containing ITO or FTO slides, was introduced to the liner. Acetic acid (6 M, 200 $\mu$L) was added, the autoclave was sealed, and the mixture was kept at 120 °C for 3 days. The resulting orange film was rinsed with anhydrous THF and dried under reduced pressure. COF bulk material that precipitated beneath the film substrate holder was filtered and purified in a Soxhlet extractor for 24 h with anhydrous THF.

**Structural Characterization.** $^1$H NMR spectra were recorded on Bruker AV 400 and AV 400 TR spectrometers. Proton chemical shifts are expressed in parts per million ($\delta$ scale) and are calibrated using residual nondeuterated solvent peaks as an internal reference (e.g., DMSO-$d_6$: 2.50 ppm). Ultraviolet−vis−infrared diffuse reflectance spectra (Kubelka−Munk spectrum) of the films were recorded on a PerkinElmer Lambda 1050 spectrometer equipped with a 150 mm integrating sphere. Thin film absorbance spectra were measured by illuminating the sample though the substrate side and correcting for reflection.[57] Scanning electron microscopy (SEM) images were recorded with a JEOL 6500F and an FEI Helios NanoLab G3 UC scanning electron microscope equipped with a field emission gun operated at 3−5 kV. Transmission electron microscopy (TEM) was performed on an FEI Titan Themis equipped with a field emission gun operated at 300 kV. X-ray diffraction (XRD) measurements were performed using a Bruker D8 Discover with Ni-filtered Cu K$\alpha$ radiation and a LynxEye position-sensitive detector. Experimental XRD data were used for Pawley refinement to optimize the hypothetical structure. The initial structure models of the COFs were built using the Forcite module of the Accelrys Materials Studio software package. We applied the space group with the highest possible symmetry, i.e., *P*6, taking into account the propeller-like conformation of the central building blocks. Using this coarse model we determined the unit cell parameters via Pawley refinement of the PXRD data. Nitrogen sorption isotherms were recorded on a Quantachrome Autosorb 1 at 77 K within a pressure range from $p/p_0$ = 0.001 to 0.98. Prior to the measurement of the sorption isotherms the samples were heated for 24 h at 120 °C under turbo-pumped vacuum. For the evaluation of the surface area the BET model was


DOI: 10.1021/jacs.7b06081
J. Am. Chem. Soc. 2018, 140, 2085−2092

applied between 0.05 and 0.2 $p/p_0$. Pore size distributions were calculated using the QSDFT equilibrium model with a carbon kernel for cylindrical pores.

## ■ ASSOCIATED CONTENT

### Supporting Information

The Supporting Information is available free of charge on the ACS Publications website at DOI: 10.1021/jacs.7b06081.

Detailed information about synthetic procedures and structural and electrochemical characterization of BDT-ETTA photoelectrodes (PDF)

## ■ AUTHOR INFORMATION


### Corresponding Authors

*bein@lmu.de

*d.fattakhova@fz-juelich.de

### ORCID

Torben Sick: 0000-0003-4684-7971

Alexander G. Hufnagel: 0000-0003-4088-937X

Paul Knochel: 0000-0001-7913-4332

Dana D. Medina: 0000-0003-4759-8612

Dina Fattakhova-Rohlfing: 0000-0003-2008-0151

Thomas Bein: 0000-0001-7248-5906


### Author Contributions

⊥T. Sick, A. G. Hufnagel, and J. Kampmann contributed equally.

### Notes

The authors declare no competing financial interest.

## ■ ACKNOWLEDGMENTS

The authors are grateful for funding from the German Science Foundation (DFG, SPP 1613), the NIM cluster (DFG), and the Free State of Bavaria (the research networks Solar Technologies Go Hybrid and UMWELTnanoTECH). The research leading to these results received funding from the European Research Council under the European Union's Seventh Framework Programme (FP7/2007-2013)/ERC Grant Agreement 321339. A.G.H. gratefully acknowledges funding by the Fonds der Chemischen Industrie. A.E. thanks the DAAD RISE worldwide program for the opportunity to conduct this research at the LMU.

## ■ REFERENCES


(1) Peter, L. M. *J. Solid State Electrochem.* **2013**, *17*, 315−326.

(2) van de Krol, R.; Liang, Y.; Schoonman, J. *J. Mater. Chem.* **2008**, *18*, 2311−2320.

(3) Sivula, K.; Le Formal, F.; Gratzel, M. *ChemSusChem* **2011**, *4*, 432−449.

(4) Dunn, H. K.; Feckl, J. M.; Muller, A.; Fattakhova-Rohlfing, D.; Morehead, S. G.; Roos, J.; Peter, L. M.; Scheu, C.; Bein, T. *Phys. Chem. Chem. Phys.* **2014**, *16*, 24610−24620.

(5) Hu, S.; Shaner, M. R.; Beardslee, J. A.; Lichterman, M.; Brunschwig, B. S.; Lewis, N. S. *Science* **2014**, *344*, 1005−1009.

(6) Reece, S. Y.; Hamel, J. A.; Sung, K.; Jarvi, T. D.; Esswein, A. J.; Pijpers, J. J.; Nocera, D. G. *Science* **2011**, *334*, 645−648.

(7) Woodhouse, M.; Parkinson, B. A. *Chem. Soc. Rev.* **2009**, *38*, 197−210.

(8) Woodhouse, M.; Parkinson, B. A. *Chem. Mater.* **2008**, *20*, 2495−2502.

(9) Singh, A. K.; Mathew, K.; Zhuang, H. L.; Hennig, R. G. *J. Phys. Chem. Lett.* **2015**, *6*, 1087−1098.

(10) Castelli, I. E.; Olsen, T.; Datta, S.; Landis, D. D.; Dahl, S.; Thygesen, K. S.; Jacobsen, K. W. *Energy Environ. Sci.* **2012**, *5*, 5814−5819.

(11) Hunt, J. R.; Doonan, C. J.; LeVangie, J. D.; Côté, A. P.; Yaghi, O. M. *J. Am. Chem. Soc.* **2008**, *130*, 11872−11873.

(12) Côte, A. P.; Benin, A. I.; Ockwig, N. W.; O'Keeffe, M.; Matzger, A. J.; Yaghi, O. M. *Science* **2005**, *310*, 1166−1170.

(13) Calik, M.; Sick, T.; Dogru, M.; Döblinger, M.; Datz, S.; Budde, H.; Hartschuh, A.; Auras, F.; Bein, T. *J. Am. Chem. Soc.* **2016**, *138*, 1234−1239.

(14) Lohse, M. S.; Rotter, J. M.; Margraf, J. T.; Werner, V.; Becker, M.; Herbert, S.; Knochel, P.; Clark, T.; Bein, T.; Medina, D. D. *CrystEngComm* **2016**, *18*, 4295−4302.

(15) Medina, D. D.; Rotter, J. M.; Hu, Y.; Dogru, M.; Werner, V.; Auras, F.; Markiewicz, J. T.; Knochel, P.; Bein, T. *J. Am. Chem. Soc.* **2015**, *137*, 1016−1019.

(16) Uribe-Romo, F. J.; Hunt, J. R.; Furukawa, H.; Klöck, C.; O'Keeffe, M.; Yaghi, O. M. *J. Am. Chem. Soc.* **2009**, *131*, 4570−4571.

(17) Chen, X.; Addicoat, M.; Irle, S.; Nagai, A.; Jiang, D. *J. Am. Chem. Soc.* **2013**, *135*, 546−549.

(18) Zhang, Y.-B.; Su, J.; Furukawa, H.; Yun, Y.; Gándara, F.; Duong, A.; Zou, X.; Yaghi, O. M. *J. Am. Chem. Soc.* **2013**, *135*, 16336−16339.

(19) Ascherl, L.; Sick, T.; Margraf, J. T.; Lapidus, S. H.; Calik, M.; Hettstedt, C.; Karaghiosoff, K.; Döblinger, M.; Clark, T.; Chapman, K. W.; Auras, F.; Bein, T. *Nat. Chem.* **2016**, *8*, 310−316.

(20) Fang, Q.; Zhuang, Z.; Gu, S.; Kaspar, R. B.; Zheng, J.; Wang, J.; Qiu, S.; Yan, Y. *Nat. Commun.* **2014**, *5*, 4503−4510.

(21) Fang, Q.; Wang, J.; Gu, S.; Kaspar, R. B.; Zhuang, Z.; Zheng, J.; Guo, H.; Qiu, S.; Yan, Y. *J. Am. Chem. Soc.* **2015**, *137*, 8352−8355.

(22) Uribe-Romo, F. J.; Doonan, C. J.; Furukawa, H.; Oisaki, K.; Yaghi, O. M. *J. Am. Chem. Soc.* **2011**, *133*, 11478−11481.

(23) Dalapati, S.; Jin, S.; Gao, J.; Xu, Y.; Nagai, A.; Jiang, D. *J. Am. Chem. Soc.* **2013**, *135*, 17310−17313.

(24) Jackson, K. T.; Reich, T. E.; El-Kaderi, H. M. *Chem. Commun.* **2012**, *48*, 8823−8825.

(25) Furukawa, H.; Yaghi, O. M. *J. Am. Chem. Soc.* **2009**, *131*, 8875−8883.

(26) Doonan, C. J.; Tranchemontagne, D. J.; Glover, T. G.; Hunt, J. R.; Yaghi, O. M. *Nat. Chem.* **2010**, *2*, 235−238.

(27) Xu, H.; Chen, X.; Gao, J.; Lin, J.; Addicoat, M.; Irle, S.; Jiang, D. *Chem. Commun.* **2014**, *50*, 1292−1294.

(28) Ding, S.-Y.; Gao, J.; Wang, Q.; Zhang, Y.; Song, W.-G.; Su, C.-Y.; Wang, W. *J. Am. Chem. Soc.* **2011**, *133*, 19816−19822.

(29) Oh, H.; Kalidindi, S. B.; Um, Y.; Bureekaew, S.; Schmid, R.; Fischer, R. A.; Hirscher, M. *Angew. Chem., Int. Ed.* **2013**, *52*, 13219−13222.

(30) Ma, H.; Ren, H.; Meng, S.; Yan, Z.; Zhao, H.; Sun, F.; Zhu, G. *Chem. Commun.* **2013**, *49*, 9773−9775.

(31) Lohse, M. S.; Stassin, T.; Naudin, G.; Wuttke, S.; Ameloot, R.; De Vos, D.; Medina, D. D.; Bein, T. *Chem. Mater.* **2016**, *28*, 626−631.

(32) DeBlase, C. R.; Silberstein, K. E.; Truong, T.-T.; Abruña, H. D.; Dichtel, W. R. *J. Am. Chem. Soc.* **2013**, *135*, 16821−16824.

(33) Chandra, S.; Kundu, T.; Kandambeth, S.; BabaRao, R.; Marathe, Y.; Kunjir, S. M.; Banerjee, R. *J. Am. Chem. Soc.* **2014**, *136*, 6570−6573.

(34) Flugel, E. A.; Lau, V. W.; Schlomberg, H.; Glaum, R.; Lotsch, B. V. *Chem. - Eur. J.* **2016**, *22*, 3676−3680.

(35) Schwinghammer, K.; Tuffy, B.; Mesch, M. B.; Wirnhier, E.; Martineau, C.; Taulelle, F.; Schnick, W.; Senker, J.; Lotsch, B. V. *Angew. Chem., Int. Ed.* **2013**, *52*, 2435−2439.

(36) Schwinghammer, K.; Mesch, M. B.; Duppel, V.; Ziegler, C.; Senker, J.; Lotsch, B. V. *J. Am. Chem. Soc.* **2014**, *136*, 1730−1733.

(37) Lau, V. W.; Mesch, M. B.; Duppel, V.; Blum, V.; Senker, J.; Lotsch, B. V. *J. Am. Chem. Soc.* **2015**, *137*, 1064−1072.

(38) Caputo, C. A.; Gross, M. A.; Lau, V. W.; Cavazza, C.; Lotsch, B. V.; Reisner, E. *Angew. Chem., Int. Ed.* **2014**, *53*, 11538−11542.

(39) Zhang, J.; Chen, X.; Takanabe, K.; Maeda, K.; Domen, K.; Epping, J. D.; Fu, X.; Antonietti, M.; Wang, X. *Angew. Chem., Int. Ed.* **2010**, *49*, 441−444.




DOI: 10.1021/jacs.7b06081
*J. Am. Chem. Soc.* 2018, 140, 2085−2092

(40) Wang, X.; Maeda, K.; Thomas, A.; Takanabe, K.; Xin, G.; Carlsson, J. M.; Domen, K.; Antonietti, M. *Nat. Mater.* **2009**, *8*, 76−80.
(41) Schwinghammer, K.; Hug, S.; Mesch, M. B.; Senker, J.; Lotsch, B. V. *Energy Environ. Sci.* **2015**, *8*, 3345−3353.
(42) Schwab, M. G.; Hamburger, M.; Feng, X.; Shu, J.; Spiess, H. W.; Wang, X.; Antonietti, M.; Mullen, K. *Chem. Commun.* **2010**, *46*, 8932−8934.
(43) Vyas, V. S.; Haase, F.; Stegbauer, L.; Savasci, G.; Podjaski, F.; Ochsenfeld, C.; Lotsch, B. V. *Nat. Commun.* **2015**, *6*, 8508−8516.
(44) Stegbauer, L.; Schwinghammer, K.; Lotsch, B. V. *Chem. Sci.* **2014**, *5*, 2789−2793.
(45) Bi, J.; Fang, W.; Li, L.; Wang, J.; Liang, S.; He, Y.; Liu, M.; Wu, L. *Macromol. Rapid Commun.* **2015**, *36*, 1799−1805.
(46) Kuecken, S.; Acharjya, A.; Zhi, L.; Schwarze, M.; Schomacker, R.; Thomas, A. *Chem. Commun. (Cambridge, U. K.)* **2017**, *53*, 5854−5857.
(47) Chen, X.; Addicoat, M.; Jin, E.; Zhai, L.; Xu, H.; Huang, N.; Guo, Z.; Liu, L.; Irle, S.; Jiang, D. *J. Am. Chem. Soc.* **2015**, *137*, 3241−3247.
(48) Haase, F.; Banerjee, T.; Savasci, G.; Ochsenfeld, C.; Lotsch, B. V. *Faraday Discuss.* **2017**, *201*, 247−264.
(49) He, S.; Rong, Q.; Niu, H.; Cai, Y. *Chem. Commun.* **2017**, *53*, 9636−9639.
(50) Banerjee, T.; Haase, F.; Savasci, G.; Gottschling, K.; Ochsenfeld, C.; Lotsch, B. V. *J. Am. Chem. Soc.* **2017**, *139*, 16228−16234.
(51) Dogru, M.; Handloser, M.; Auras, F.; Kunz, T.; Medina, D.; Hartschuh, A.; Knochel, P.; Bein, T. *Angew. Chem., Int. Ed.* **2013**, *52*, 2920−2924.
(52) Calik, M.; Auras, F.; Salonen, L. M.; Bader, K.; Grill, I.; Handloser, M.; Medina, D. D.; Dogru, M.; Löbermann, F.; Trauner, D.; Hartschuh, A.; Bein, T. *J. Am. Chem. Soc.* **2014**, *136*, 17802−17807.
(53) (a) Medina, D. D.; Werner, V.; Auras, F.; Tautz, R.; Dogru, M.; Schuster, J.; Linke, S.; Döblinger, M.; Feldmann, J.; Knochel, P.; Bein, T. *ACS Nano* **2014**, *8*, 4042−4052. (b) Medina, D. D.; Petrus, M. L.; Jumabekov, A. N.; Margraf, J. T.; Weinberger, S.; Rotter, J. M.; Clark, T.; Bein, T. *ACS Nano* **2017**, *11*, 2706−2713.
(54) Jin, S.; Ding, X.; Feng, X.; Supur, M.; Furukawa, K.; Takahashi, S.; Addicoat, M.; El-Khouly, M. E.; Nakamura, T.; Irle, S.; Fukuzumi, S.; Nagai, A.; Jiang, D. *Angew. Chem., Int. Ed.* **2013**, *52*, 2017−2021.
(55) Zhou, T. Y.; Xu, S. Q.; Wen, Q.; Pang, Z. F.; Zhao, X. *J. Am. Chem. Soc.* **2014**, *136*, 15885−15888.
(56) Sathre, R.; Scown, C. D.; Morrow, W. R.; Stevens, J. C.; Sharp, I. D.; Ager, J. W.; Walczak, K.; Houle, F. A.; Greenblatt, J. B. *Energy Environ. Sci.* **2014**, *7*, 3264−3278.
(57) Klahr, B. M.; Martinson, A. B. F.; Hamann, T. W. *Langmuir* **2011**, *27*, 461−468.


DOI: 10.1021/jacs.7b06081
*J. Am. Chem. Soc.* 2018, 140, 2085−2092